THE JOURNAL OF PHYSICAL CHEMISTRY Letters

Letter

pubs.acs.org/JPCL

Addressing Colloidal Stability for Unambiguous Electroanalysis of Single Nanoparticle Impacts

Donald A. Robinson, Aditya M. Kondajji, Alma D. Castañeda, Radhika Dasari, Richard M. Crooks, and Keith J. Stevenson*,†

Department of Chemistry, Center for Nano- and Molecular Science, and Center for Electrochemistry, University of Texas at Austin, Austin, Texas 78712, United States

Supporting Information

ABSTRACT: Herein the problem of colloidal instability on electrochemically detected nanoparticle (NP) collisions with a Hg ultramicroelectrode (UME) by electrocatalytic amplification is addressed. NP tracking analysis (NTA) shows that rapid aggregation occurs in solution after diluting citrate-stabilized Pt NPs with hydrazine/phosphate buffers of net ionic strength greater than 70 mM. Colloidal stability improves by lowering the ionic strength, indicating that aggregation processes were strongly affected by charge screening of the NP double layer interactions at high cation concentrations. For the system of lowest ionic strength, the overwhelming majority of observed electrocatalytic current signals represent single NP/electrode impacts, as confirmed by NTA kinetic monitoring. NP diffusion coefficients determined by NTA and NP impact electroanalysis are in excellent agreement for the stable colloids, which signifies that the sticking probability of Pt NPs interacting with Hg is unity and that the observed NP impact rate agrees with the expected steady-state diffusive flux expression for the spherical cap Hg UME.

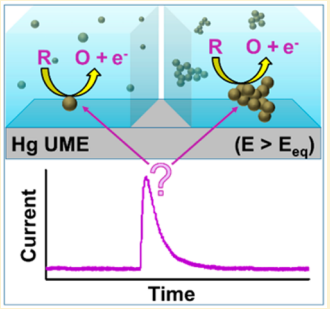

Nanoparticle impact electroanalysis (NIE) is an emerging methodology for electrochemical characterization of single nanoparticles (NPs) and in the development of ultralow detection sensors for a host of analytes. We broadly define NIE as any method based on the electrochemical detection of discrete NPs in solution as they collide with the surface of an electrode.[1−7] The ability to probe individual microscopic particles in solution with ultramicroelectrodes (UMEs) has inspired fundamental studies of single NP electrochemistry and NP/electrode interactions,[8−17] diffusive and electro/magnetophoretic particle transport,[18−22] and the development of electrochemical bioassays with single-molecule sensitivity.[23,24] Colloidal stability[25,26] is of critical importance for the accurate interpretation of NP/electrode impacts. Many previous interpretations of NIE data were based on the assumption that the NPs remain stable after transfer from a pure aqueous or as-synthesized medium to the test electrolyte solution. However, to the best of our knowledge, this assumption has not been tested by NP size/concentration monitoring across the time scale of the NIE experiment (typically 5−10 min). The ultimate goal of this investigation is to establish a stable NIE system wherein the observed current transients can be safely interpreted to result from single NPs upon impact with the UME.

Colloidal instability and its effects on the analysis of NP/electrode impacts have been explored recently by a few groups working on different NIE systems. Alpuche-Aviles and co-workers employed dynamic light scattering (DLS) for colloidal characterization of dye-sensitized TiO_2 NP aggregates that were detected based on the photocatalytic oxidation of methanol and subsequent charge transfer upon impact with a fluorine-doped tin oxide (FTO) UME.[27] Compton and co-workers found that high concentrations of sodium citrate (0.1 M) stabilize Ag NPs according to accumulated charge from Ag oxidation and correlation to NP sizes measured by scanning electron microscopy (SEM).[28] Compton later investigated the flocculation of Ag NPs in solutions of varied KCl concentrations[29] by DLS and nanoparticle tracking analysis (NTA).[30−32] For NPs dispersed in KCl concentrations greater than 20 mM, the authors noticed a large difference between the measured NP size distributions from DLS and NTA in comparison to that calculated from measured charge of each impact. This difference was attributed to the ability of the NP impact method to differentiate between irreversible aggregates and reversible agglomerates in solution.[29] Most relevant to the present study, however, is the work of Koper and co-workers,[33] who discovered evidence of aggregation in a NIE system based on electrocatalytic amplification (ECA), a detection strategy first demonstrated by Bard and co-workers.[1,2] The ECA method for sensing individual NP/electrode collisions relies on the detection of a burst of current when a NP strikes an inert UME and catalyzes the oxidation or reduction of active molecules in solution. Based on observations from NIE, cyclic voltammetry, and electron microscopy, the authors proposed that Pt NPs aggregated upon exposure to ECA solutions because of reactions between N_2H_4, the redox-active molecule,

Received: May 24, 2016
Accepted: June 15, 2016
Published: June 16, 2016

ACS Publications © 2016 American Chemical Society

DOI: 10.1021/acs.jpclett.6b01131
J. Phys. Chem. Lett. 2016, 7, 2512−2517

and the Pt surface; specifically the chemisorption of N_2H_4 on Pt possibly followed by desorption of stabilizing citrate ligands.[33]

Our own groups have characterized hybrid Pt-decorated iron oxide NPs (Pt-IONPs) using NTA[22] and showed that the as-synthesized Pt-IONPs were suspended as aggregates in deionized water and maintained their average hydrodynamic size after exposure to 15 mM N_2H_4 and 50 mM phosphate buffer. We found that the resulting rate of Pt-IONP impacts (impact frequency as a function of particle concentration)[2] with a Au disk UME agreed well with theoretical predictions of diffusion-limited transport based on particle sizing and quantification by NTA, in contrast to previous reports of citrate-capped Pt NPs in comparable ECA solution conditions.[2,34] Very recently, Kanoufi, Tessier, and co-workers developed an *in situ* approach for correlated electrochemical and optical detection of Ag NP impacts.[35] The authors reported 22 optically detected Ag NP landings onto a transparent Au UME over a 700 s time period, only 10 of which were detectable by simultaneously recorded current spikes for Ag NP oxidation. The optically detected impact events occurred at the expected diffusion-limited rate for the UME geometry. Several groups have reported Na^+ or K^+ molarities ranging from 30 to 50 mM as the critical concentration of coagulation for 50−70 nm citrate-stabilized Ag NPs,[36−39] so colloidal stability in these experiments may not be suitable for such an analysis.

To the best of our knowledge, a linear calibration curve relating the frequency of observed impact events to concentration of citrate-capped noble metal NPs has not yet been reported to give the expected rate based on diffusion-limited flux to the UME surface. Previous experimentally determined ECA impact rates involving citrate-stabilized Pt NPs and N_2H_4 have been found to be much slower than predicted[2,34] if one assumes that diffusion-limited transport dominates the frequency of observed NP impacts and that the colloidal sample is stable with unchanging NP size/concentration. For the following experiments, time-resolved NTA[30−32] was used to monitor changes in NP size and concentration, which made it possible to systematically interrogate the rapid diffusion-limited[33,40] aggregation kinetics of Pt NPs under different solution conditions. Direct comparison of data from the NTA and NIE experiments provided fundamental insight into how colloidal interactions affect the analysis of NP/electrode impacts. This information served to guide optimization of experimental conditions necessary for stabilizing a monodispersed Pt NP sample and ultimately allows us to confidently interpret ECA signals as truly representing single, not aggregated, NP impact events. Impact rates were then found to agree with prediction based solely on diffusion, as confirmed by calibration of impact frequency to NP concentration and comparison of NIE-derived diffusion coefficient with that estimated by SEM sizing and the Stokes−Einstein−Sutherland relation[41,42] (eq S1 of the Supporting Information).

Commonly used solution conditions for ECA-based sensing of NP impacts involve mixtures of 10−15 mM N_2H_4 redox indicator with 10−50 mM phosphate buffer as the supporting electrolyte.[2,43−47] Accordingly, we adopted similar solution conditions as a starting point for our studies (see Supporting Information for supplemental discussion). The Pt NPs in this study were synthesized for compatibility with NTA to have a diameter of 50 ± 10 nm as measured by SEM (Figure S1, Supporting Information).[48] Because N_2H_4 had already been determined to act as a coagulant for 3−5 nm citrate-capped Pt NPs,[33] we first investigated the effect of sodium phosphate buffer (SPB) on colloidal stability. As shown in Figure S2, the hydrodynamic size distribution of Pt NPs in 40 mM SPB (pH 7.8) is similar to that of the sample suspended in water alone, 60 ± 20 nm, which indicates that SPB does not disrupt colloidal stability in the absence of N_2H_4. By contrast, the Pt NPs in 25 mM SPB + 10 mM N_2H_4 (pH 7.8) have an average diameter of 80 ± 40 nm. Interestingly, the 25 mM SPB solution containing N_2H_4 has a calculated ionic strength of 70 mM, while that of the 40 mM SPB solution is higher (100 mM). This result confirms that coagulation is not brought about by the pH buffer alone at ionic strength less than 0.1 M and that N_2H_4 does indeed play a significant role in Pt NP aggregation. Figure S3 is a 3D plot resulting from kinetic NTA measurements that compares the concentration and size of 50 nm Pt NPs in 50 mM SPB (pH 7.8) + 10 mM N_2H_4 for 12 min. This solution condition is the highest ionic strength of all samples tested, so it is expected to aggregate the fastest. Corresponding two-dimensional (2-D) plots of concentration and size as a function of time are included in Figure S4 of the Supporting Information for a more detailed representation of the distributions. The NTA plots show that the overall NP concentration decreases significantly with time, while the size distribution simultaneously increases, indicating Pt coagulation. The NP concentration decreases to roughly half of the initial concentration ($C_{NP,0}$ = 1.1 pM) ∼ 100 s after NP mixing, while the mean NP diameter nearly doubles in size by the end of the 700 s analysis time. Importantly, as shown in Figure S4c, the changing NTA size distributions at four discrete time intervals reveal that the NP size distribution becomes more polydisperse and includes diameters larger than 400 nm in the minority population after the total time scale of the analysis.

Because charge-screening is also expected to play a significant physical role in NP aggregation processes, the stability of the NPs in phosphate buffers of varied ionic strengths was investigated with NTA. As shown in Figure 1, the kinetic changes in both NP size and concentration are strongly influenced by the net ionic strength of the buffer in the presence of 10 mM N_2H_4. The ionic strength of the 0 mM SPB

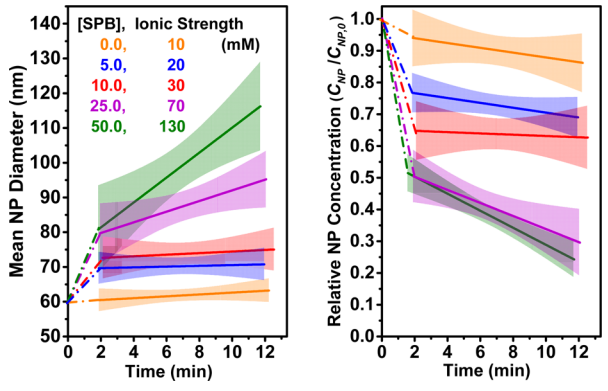

Figure 1. Fitted linear trends of mean hydrodynamic diameter (left panel) and relative concentration (right panel) of dilute Pt colloids as determined by NTA. Each plot corresponds to samples containing 10 mM N_2H_4 and different sodium phosphate buffer concentration, [SPB], at pH 7.8. Colored transparent regions are 95% confidence level bands for regression analysis of raw NTA scatter data; dashed lines are extrapolations to expected initial values from NTA in pure water. Time zero marks when a small aliquot of stock Pt NPs is mixed with N_2H_4/SPB solution.

DOI: 10.1021/acs.jpclett.6b01131
J. Phys. Chem. Lett. 2016, 7, 2512−2517

sample is approximately 10 mM; this is because hydrazine itself is a weak base, pK_a = 8.1 for $N_2H_4/N_2H_5^+$.[49] To clarify, the 0 mM SPB sample was prepared by adjusting the pH of an aqueous N_2H_4 to pH 7.8 with H_2SO_4, resulting in a hydrazine sulfate buffer. The size distributions for Figure 1 span a large range as shown in more detail by the corresponding scatter plots in Figure S5 of the Supporting Information. The predominant evidence of rapid aggregation is observed for 25 and 50 mM SPB samples, considering both the NP concentration depletion kinetics and rate of particle growth (Figure 1). By contrast, the Pt NP solution without SPB stays at a consistent concentration and average size over the analysis time, indicating that the colloid remains sufficiently stable in 10 mM hydrazine sulfate. Slight aggregation is indicated for the 5 mM and 10 mM SPB samples according to the difference in overall NP diameter and concentration when compared to values measured in pure water or 10 mM hydrazine sulfate alone. The relative increase in NP diameter is roughly +17 and +25% with the corresponding decrease in NP concentration being about −23 and −37% of the initial NP concentration at time zero ($C_{NP,0}$) for the 5 and 10 mM SPB conditions, respectively. Taking into consideration the observed variance of NTA measurements and inherent bias toward tracking larger NPs more accurately due to higher scattering intensities, we surmise that the solution conditions involving SPB concentrations ≤10 mM were sufficiently optimized so that the overwhelming majority of the NPs maintain suitable colloidal stability for NIE of single Pt NPs.

Our group has previously reported on the optimization of electrode materials, Hg in particular, to enhance signal-to-noise and improve time resolution of the ECA response for NP impacts.[43−46] The fundamental principles of our detection strategy are illustrated in Figure 2. No current is observed prior

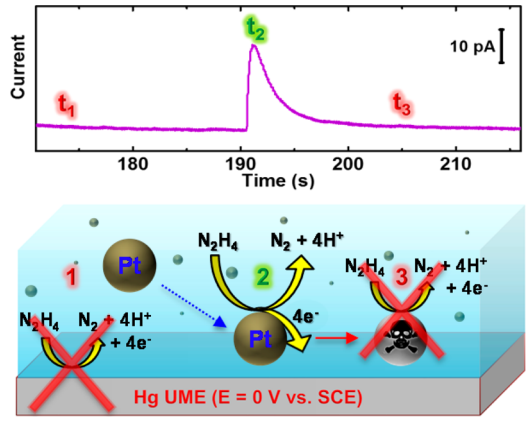

Figure 2. Current vs time trace of ECA current spike corresponding to a single Pt NP impact on Hg UME with schematic representation included in the bottom panel.

to NP impact (t_1), because the UME, Hg in this case, does not oxidize the redox probe, N_2H_4, present in solution at the applied potential (0 V vs SCE). At the moment of impact (t_2), however, the single colliding Pt NP acts as a nanoelectrode for the electrocatalytic oxidation of N_2H_4. This gives rise to a sharp current spike, followed by a slower decay that results from Hg poisoning of the catalytic Pt NP surface (t_3).[43−46] The current then completely returns to baseline if no other NPs collide with the Hg UME during the Pt surface deactivation time ($t_3 - t_2$).

The electrochemical NP impact method is sensitive to changes in the bulk particle concentration and size distribution, which establishes NIE as another viable method for reporting on NP aggregation kinetics. Representative CA traces of ECA collision events for three different buffer conditions are shown in Figure 3 and Figure S6 of the Supporting Information for

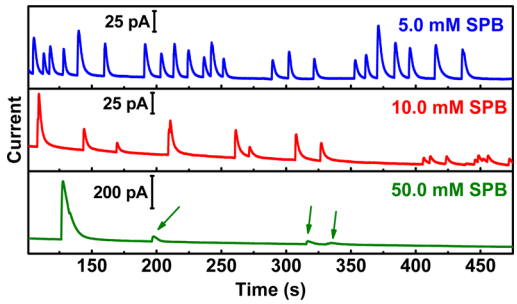

Figure 3. CA traces of current responses for NP impacts on Hg/Pt UME in three different phosphate buffer concentrations with 230 fM Pt NPs in 10 mM N_2H_4, pH 7.8. Green arrows point to positions of smaller transient current signals.

230 fM and 1.1 pM Pt NPs, respectively. Both sets of CA traces present the same relative trend of decreased NIE signal frequency in higher ionic strengths. Much larger NIE signals in terms of both current magnitude and Hg deactivation time are observed for the 50 mM SPB sample, indicating the electrode impacts of large NP aggregates. We infer that the 400 pA collision event shown at ∼130 s may correspond to an aggregate, while the three small signals around 200, 320 and 335 s are more likely to represent NIE response of individual 50 nm Pt NPs (Figure 3, green trace). At higher Pt NP concentrations, a more pronounced aggregation effect is observed for the 50 mM SPB sample, displaying very large/broad NIE signals that complicate the analysis of smaller impacts (Figure S6, Supporting Information). At the lowest ionic strength, the impact signal frequency and amplitude remain relatively consistent throughout the recorded time period, indicating that Pt NP size does not change very much over the time scale of the analysis because conditions are favorable for colloidal stability.

NIE signal frequencies were analyzed at varied Pt NP concentrations (Figure 4) to understand the effect of aggregation on NP transport to the UME/solution interface. The overall NP/UME impact frequency is expected to be directly proportional to both NP concentration and average diffusion coefficient according to diffusion-limited transport to the spherical cap Hg UME (eq 1).

$$R_{NP} = f_{NP} C_{NP}^{-1} = 2\pi\beta N_A D_{NP} a_{UME} \quad (1)$$

Here R_{NP} represents the rate at which NPs collide with the Hg UME, f_{NP} is the frequency of NP impacts at a given NP concentration (C_{NP}), N_A is Avogadro's number, D_{NP} is the NP diffusion coefficient, and a is the basal radius of the Hg spherical cap (5 μm for Pt disk UME substrate). The term β is a size dependent constant for the superhemispherical cap family of UMEs based on the calculations by Alfred and Oldham.[50] The Hg UME was reproducibly grown as superhemispherical with surface area that is on average 1.84-fold larger than a perfect hemisphere with 5 μm radius, giving a β value of 1.35 (Figure S7, Supporting Information).

DOI: 10.1021/acs.jpclett.6b01131
J. Phys. Chem. Lett. 2016, 7, 2512−2517

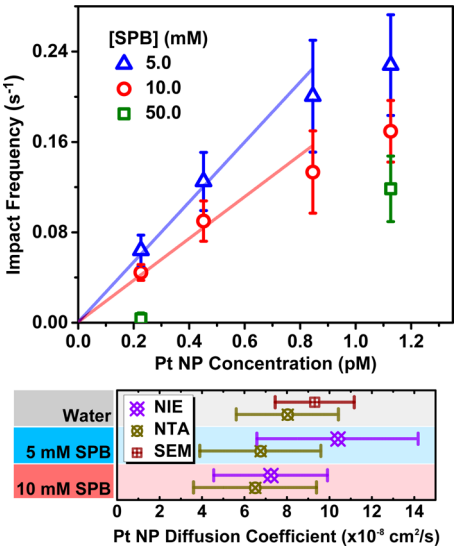

Figure 4. NP impact rate analysis. Top panel: impact event frequency (event counts per 400 s sampling from 15 to 415 s post mixing) plotted with respect to NP concentration in the presence of 10 mM N_2H_4 with different SPB concentrations; vertical bars are standard error of 5 replicate NIE measurements. Bottom panel: NP diffusion coefficients approximated from SEM, NIE, and NTA.

According to eq 1, the NP impact frequency is proportional to C_{NP} and D_{NP}, both of which decrease over time for an aggregating Pt NP sample. As shown in Figure 4a, the NP impact frequency is inversely proportional to ionic strength, which correlates to the same general trend of NP concentration as monitored by NTA (Figure 1). For a stable dispersed colloid, f_{NP} should increase linearly with NP concentration.[22] Linear calibration curves were established for the two lower ionic strength conditions in Figure 4a. The difference in the slope between the 5 and 10 mM SPB samples (blue and red curves) indicates their relative stabilities, with the 5 mM condition being most stable. The limit of detection for the 5 mM SPB condition is 160 fM Pt NP for a 400 s CA acquisition time. As shown in Figure 4b, the calculated NP diffusion coefficients based on the NIE slope (R_{NP}, eq 1) for the two optimized systems of lower ionic strength correlate well with NTA for Pt NP samples measured under identical solution conditions and in deionized water. Shown for further comparison is the calculated D_{NP} from eq S1 using diameters of individual Pt NPs measured by SEM, which also lies within the range of error for the NIE experiments. The collision rates obtained in previous studies of 3−4 nm Pt NPs by Bard and co-workers were calculated to correspond to an apparent diffusion coefficient of $\sim 1 \times 10^{-8}$ cm^2/s.[2] This value is 1 order of magnitude slower than what we obtain here for NPs that are 10 times larger in diameter. We suspect that the reason for the previously reported D_{NP} value is likely due to rapid NP aggregation because experiments involved unoptimized solution conditions (e.g., 50 mM phosphate buffer and 15 mM N_2H_4) that do not support citrate-stabilized Pt colloids.[33] The previously proposed kinetic limitations on observed NP impact event frequency for this system[34] should therefore be reconsidered with the inclusion of colloidal instability effects. For the optimized 50 nm Pt colloids, however, the unprecedented agreement of the NIE system with NTA and SEM characterizations confirms that the observed ECA signals resulted from single NP impacts on a Hg UME.

In summary, fast aggregation of 50 nm citrate-stabilized Pt NPs ensues when the ionic strength of the hydrazine/phosphate buffer is ≥70 mM. The colloidal stability is maintained at ionic strengths <20 mM if Pt NP concentrations are kept lower than 1.1 pM. We conclude that the overall cause of coagulation/aggregation for our systems is brought about by two general processes: (1) the chemically induced instability specifically from N_2H_4 reactivity with Pt as previously proposed by Koper (the intricate details of this mechanism are currently under investigation and will be reported in due course) and (2) the instability at higher electrolyte concentrations, consistent with the well-known Schulze-Hardy rule and DLVO theory of interparticle electrostatic double-layer and van der Waals interactions.[25] The effect of specific N_2H_4/Pt chemical interactions was not found to significantly contribute to NP aggregation at lower ionic strengths, although we did confirm that N_2H_4 does actively participate as a chemical coagulant if electrostatic colloidal stabilization becomes compromised by the concentration of cations (Na^+, $N_2H_5^+$) in solution. When solution and NP parameters are optimized to prevent aggregation, the Pt NPs collide with the Hg/Pt UME at the expected average rate according to NTA experiments and theoretical predictions based on diffusion-limited transport of individual NPs to a UME surface. The experimental/theoretical agreement indicates that each single NP impact leads to an observable ECA current response, signifying that the sticking probability of the NP/UME interaction is essentially unity for collision with the Hg surface, which contrasts with previously proposed theory[34] for Pt NP collisions on Au UME detected using hydrazine. Such efficient NP sticking behavior is expected for the UME because of Hg's well-known properties of rapidly wetting Pt upon physical contact[51] due to surface/subsurface alloying.[43,52] Because the resulting NP/UME collision rates for the optimized Pt NP samples are in agreement with theory of diffusion-limited NP transport, we conclude that each Pt NP becomes immediately wetted by the liquid metal upon impact with the Hg UME, therefore making direct electrical contact and an observable ECA current spike. This sets the Hg UME experimental setup (with colloidally stable Pt NPs) apart from other NIE systems in terms of efficiency for detecting multiple NP impacts over time, where predictions based on steady-state diffusive flux equations have previously been found to disagree with experimentally determined impact frequencies[2,4] and in situ optical experiments of Ag NP electrodissolution on a UME.[35] Our carefully controlled Pt NP and Hg UME experimental setup gives results that agree well with the same mathematical relationships based on Fick's Laws of Diffusion that are generally used to model steady-state diffusion-limited current from electrolysis of small molecules,[50] establishing a correlation between ensemble (diffusion-limited current from small molecule electrochemistry) and digitized (frequency of single NP impacts) electroanalysis, as further supported by our earlier findings for stable Pt-decorated iron oxide NP aggregates without the presence of a magnetic field.[22]

The combined results of the NIE and NTA colloidal characterizations in the optimized experiments confirm that observed electrochemical signals using phosphate-buffered 10 mM N_2H_4 solutions of <20 mM ionic strength are predominantly the result of electrocatalytic hydrazine oxidation on individually dispersed 50 nm Pt NPs after colliding with a Hg UME. The establishment of quantitative correlations between NIE and NTA is currently underway to develop cross-correlative analytical standards, which will significantly aid

DOI: 10.1021/acs.jpclett.6b01131
J. Phys. Chem. Lett. 2016, 7, 2512−2517

in ongoing pursuits to develop NIE for applications such as colloidal NP size characterizations,[43] evaluations of catalytic activities at the single NP level,[11,13] and strategies for ultrasensitive bioanalysis.[23]

■ ASSOCIATED CONTENT

Supporting Information

The Supporting Information is available free of charge on the ACS Publications website at DOI: 10.1021/acs.jpclett.6b01131.

Experimental details, SEM of Pt NPs, additional NTA plots and CA traces of NP impact events, optical micrograph of Hg/Pt UME, supplemental discussion and references (PDF)

■ AUTHOR INFORMATION

Corresponding Author

*E-mail: K.Stevenson@skoltech.ru.

Present Address

†Skolkovo Institute of Science and Technology, Center for Electrochemical Energy Storage, 3 Nobel Street, Moscow 143026, Russia.

Notes

The authors declare no competing financial interest.

■ ACKNOWLEDGMENTS

We thank the Defense Threat Reduction Agency (DTRA) (Grant HDTRA1-11-1-0005) for financial support. D.A.R. acknowledges X. Chen for courteous assistance with NTA and J. Duay, T. Alligrant, and A. Boika for preliminary experiments and helpful discussions.

■ REFERENCES

(1) Xiao, X.; Bard, A. J. Observing Single Nanoparticle Collisions at an Ultramicroelectrode by Electrocatalytic Amplification. *J. Am. Chem. Soc.* **2007**, *129*, 9610−9612.

(2) Xiao, X.; Fan, F.-R. F.; Zhou, J.; Bard, A. J. Current Transients in Single Nanoparticle Collision Events. *J. Am. Chem. Soc.* **2008**, *130*, 16669−16677.

(3) Bard, A. J.; Zhou, H.; Kwon, S. J. Electrochemistry of Single Nanoparticles via Electrocatalytic Amplification. *Isr. J. Chem.* **2010**, *50*, 267−276.

(4) Kleijn, S. E. F.; Lai, S. C. S.; Koper, M. T. M.; Unwin, P. R. Electrochemistry of Nanoparticles. *Angew. Chem., Int. Ed.* **2014**, *53*, 3558−3586.

(5) Cheng, W.; Compton, R. G. Electrochemical Detection of Nanoparticles by 'Nano-Impact' Methods. *TrAC, Trends Anal. Chem.* **2014**, *58*, 79−89.

(6) Wang, W.; Tao, N. Detection, Counting, and Imaging of Single Nanoparticles. *Anal. Chem.* **2014**, *86*, 2−14.

(7) Oja, S. M.; Fan, Y.; Armstrong, C. M.; Defnet, P.; Zhang, B. Nanoscale Electrochemistry Revisited. *Anal. Chem.* **2016**, *88*, 414−430.

(8) Xiao, X.; Pan, S.; Jang, J. S.; Fan, F.-R. F.; Bard, A. J. Single Nanoparticle Electrocatalysis: Effect of Monolayers on Particle and Electrode on Electron Transfer. *J. Phys. Chem. C* **2009**, *113*, 14978−14982.

(9) Zhou, H.; Fan, F.-R. F.; Bard, A. J. Observation of Discrete Au Nanoparticle Collisions by Electrocatalytic Amplification Using Pt Ultramicroelectrode Surface Modification. *J. Phys. Chem. Lett.* **2010**, *1*, 2671−2674.

(10) Zhou, Y.-G.; Rees, N. V.; Compton, R. G. The Electrochemical Detection and Characterization of Silver Nanoparticles in Aqueous Solution. *Angew. Chem., Int. Ed.* **2011**, *50*, 4219−4221.

(11) Kleijn, S. E. F.; Lai, S. C. S.; Miller, T. S.; Yanson, A. I.; Koper, M. T. M.; Unwin, P. R. Landing and Catalytic Characterization of Individual Nanoparticles on Electrode Surfaces. *J. Am. Chem. Soc.* **2012**, *134*, 18558−18561.

(12) Kim, J.; Kim, B.-K.; Cho, S. K.; Bard, A. J. Tunneling Ultramicroelectrode: Nanoelectrodes and Nanoparticle Collisions. *J. Am. Chem. Soc.* **2014**, *136*, 8173−8176.

(13) Guo, Z.; Percival, S. J.; Zhang, B. Chemically Resolved Transient Collision Events of Single Electrocatalytic Nanoparticles. *J. Am. Chem. Soc.* **2014**, *136*, 8879−8882.

(14) Ly, L. S. Y.; Batchelor-McAuley, C.; Tschulik, K.; Kätelhön, E.; Compton, R. G. A Critical Evaluation of the Interpretation of Electrocatalytic Nanoimpacts. *J. Phys. Chem. C* **2014**, *118*, 17756−17763.

(15) Chen, C.-H.; Ravenhill, E. R.; Momotenko, D.; Kim, Y.-R.; Lai, S. C. S.; Unwin, P. R. Impact of Surface Chemistry on Nanoparticle−Electrode Interactions in the Electrochemical Detection of Nanoparticle Collisions. *Langmuir* **2015**, *31*, 11932−11942.

(16) Castañeda, A. D.; Alligrant, T. M.; Loussaert, J. A.; Crooks, R. M. Electrocatalytic Amplification of Nanoparticle Collisions at Electrodes Modified with Polyelectrolyte Multilayer Films. *Langmuir* **2015**, *31*, 876−885.

(17) Percival, S. J.; Zhang, B. Fast-Scan Cyclic Voltammetry Allows Determination of Electron-Transfer Kinetic Constants in Single Nanoparticle Collision. *J. Phys. Chem. C* **2016**, DOI: 10.1021/acs.jpcc.5b11330.

(18) Boika, A.; Thorgaard, S. N.; Bard, A. J. Monitoring the Electrophoretic Migration and Adsorption of Single Insulating Nanoparticles at Ultramicroelectrodes. *J. Phys. Chem. B* **2013**, *117*, 4371−4380.

(19) Park, J. H.; Boika, A.; Park, H. S.; Lee, H. C.; Bard, A. J. Single Collision Events of Conductive Nanoparticles Driven by Migration. *J. Phys. Chem. C* **2013**, *117*, 6651−6657.

(20) Yoo, J. J.; Anderson, M. J.; Alligrant, T. M.; Crooks, R. M. Electrochemical Detection of Insulating Beads at Subattomolar Concentration via Magnetic Enrichment in a Microfluidic Device. *Anal. Chem.* **2014**, *86*, 4302−4307.

(21) Boika, A.; Bard, A. J. Time of First Arrival in Electrochemical Collision Experiments as a Measure of Ultralow Concentrations of Analytes in Solution. *Anal. Chem.* **2015**, *87*, 4341−4346.

(22) Robinson, D. A.; Yoo, J. J.; Castañeda, A. D.; Gu, B.; Dasari, R.; Crooks, R. M.; Stevenson, K. J. Increasing the Collision Rate of Particle Impact Electroanalysis with Magnetically Guided Pt-Decorated Iron Oxide Nanoparticles. *ACS Nano* **2015**, *9*, 7583−7595.

(23) Alligrant, T. M.; Nettleton, E. G.; Crooks, R. M. Electrochemical Detection of Individual DNA Hybridization Events. *Lab Chip* **2013**, *13*, 349−354.

(24) Dick, J. E.; Hilterbrand, A. T.; Boika, A.; Upton, J. W.; Bard, A. J. Electrochemical Detection of a Single Cytomegalovirus at an Ultramicroelectrode and Its Antibody Anchoring. *Proc. Natl. Acad. Sci. U. S. A.* **2015**, *112*, 5303−5308.

(25) Verwey, E. J. W.; Overbeek, J. T. G. *Theory of the Stability of Lyophobic Colloids*; Elsevier Publishing Company, Inc.: New York, 1999.

(26) Sinha, P.; Szilagyi, I.; Montes Ruiz-Cabello, F. J.; Maroni, P.; Borkovec, M. Attractive Forces between Charged Colloidal Particles Induced by Multivalent Ions Revealed by Confronting Aggregation and Direct Force Measurements. *J. Phys. Chem. Lett.* **2013**, *4*, 648−652.

(27) Fernando, A.; Chhetri, P.; Barakoti, K. K.; Parajuli, S.; Kazemi, R.; Alpuche-Aviles, M. A. Transient Interactions of Agglomerates of Sensitized TiO_2 Nanoparticles in Colloidal Suspensions. *J. Electrochem. Soc.* **2016**, *163*, H3025−H3031.

(28) Lees, J. C.; Ellison, J.; Batchelor-McAuley, C.; Tschulik, K.; Damm, C.; Omanović, D.; Compton, R. G. Nanoparticle Impacts Show High-Ionic-Strength Citrate Avoids Aggregation of Silver Nanoparticles. *ChemPhysChem* **2013**, *14*, 3895−3897.

(29) Sokolov, S. V.; Tschulik, K.; Batchelor-McAuley, C.; Jurkschat, K.; Compton, R. G. Reversible or Not? Distinguishing Agglomeration

DOI: 10.1021/acs.jpclett.6b01131
J. Phys. Chem. Lett. 2016, 7, 2512−2517

and Aggregation at the Nanoscale. *Anal. Chem.* **2015**, *87*, 10033−10039.
(30) Malloy, A.; Carr, B. Nanoparticle Tracking Analysis - the Halo™ System. *Part. Part. Syst. Charact.* **2006**, *23*, 197−204.
(31) Filipe, V.; Hawe, A.; Jiskoot, W. Critical Evaluation of Nanoparticle Tracking Analysis (NTA) by Nanosight for the Measurement of Nanoparticles and Protein Aggregates. *Pharm. Res.* **2010**, *27*, 796−810.
(32) Axson, J. L.; Stark, D. I.; Bondy, A. L.; Capracotta, S. S.; Maynard, A. D.; Philbert, M. A.; Bergin, I. L.; Ault, A. P. Rapid Kinetics of Size and Ph-Dependent Dissolution and Aggregation of Silver Nanoparticles in Simulated Gastric Fluid. *J. Phys. Chem. C* **2015**, *119*, 20632−20641.
(33) Kleijn, S. E. F.; Serrano-Bou, B.; Yanson, A. I.; Koper, M. T. M. Influence of Hydrazine-Induced Aggregation on the Electrochemical Detection of Platinum Nanoparticles. *Langmuir* **2013**, *29*, 2054−2064.
(34) Kwon, S. J.; Zhou, H.; Fan, F.-R. F.; Vorobyev, V.; Zhang, B.; Bard, A. J. Stochastic Electrochemistry with Electrocatalytic Nanoparticles at Inert Ultramicroelectrodes-Theory and Experiments. *Phys. Chem. Chem. Phys.* **2011**, *13*, 5394−5402.
(35) Brasiliense, V.; Patel, A. N.; Martinez-Marrades, A.; Shi, J.; Chen, Y.; Combellas, C.; Tessier, G.; Kanoufi, F. Correlated Electrochemical and Optical Detection Reveals the Chemical Reactivity of Individual Silver Nanoparticles. *J. Am. Chem. Soc.* **2016**, *138*, 3478−3483.
(36) Huynh, K. A.; Chen, K. L. Aggregation Kinetics of Citrate and Polyvinylpyrrolidone Coated Silver Nanoparticles in Monovalent and Divalent Electrolyte Solutions. *Environ. Sci. Technol.* **2011**, *45*, 5564−5571.
(37) Li, X.; Lenhart, J. J.; Walker, H. W. Aggregation Kinetics and Dissolution of Coated Silver Nanoparticles. *Langmuir* **2012**, *28*, 1095−1104.
(38) Gicheva, G.; Yordanov, G. Removal of Citrate-Coated Silver Nanoparticles from Aqueous Dispersions by Using Activated Carbon. *Colloids Surf., A* **2013**, *431*, 51−59.
(39) Gutierrez, L.; Aubry, C.; Cornejo, M.; Croue, J.-P. Citrate-Coated Silver Nanoparticles Interactions with Effluent Organic Matter: Influence of Capping Agent and Solution Conditions. *Langmuir* **2015**, *31*, 8865−8872.
(40) Lin, M. Y.; Lindsay, H. M.; Weitz, D. A.; Klein, R.; Ball, R. C.; Meakin, P. Universal Diffusion-Limited Colloid Aggregation. *J. Phys.: Condens. Matter* **1990**, *2*, 3093−3113.
(41) Sutherland, W. A Dynamical Theory of Diffusion for Non-Electrolytes and the Molecular Mass of Albumin. *Philos. Mag. Ser. 6* **1905**, *9*, 781−785.
(42) Einstein, A. *Investigations on the Theory of the Brownian Movement*; Dover Publications, Inc.: New York, 1956.
(43) Dasari, R.; Robinson, D. A.; Stevenson, K. J. Ultrasensitive Electroanalytical Tool for Detecting, Sizing, and Evaluating the Catalytic Activity of Platinum Nanoparticles. *J. Am. Chem. Soc.* **2013**, *135*, 570−573.
(44) Dasari, R.; Walther, B.; Robinson, D. A.; Stevenson, K. J. Influence of the Redox Indicator Reaction on Single-Nanoparticle Collisions at Mercury- and Bismuth-Modified Pt Ultramicroelectrodes. *Langmuir* **2013**, *29*, 15100−15106.
(45) Dasari, R.; Tai, K.; Robinson, D. A.; Stevenson, K. J. Electrochemical Monitoring of Single Nanoparticle Collisions at Mercury-Modified Platinum Ultramicroelectrodes. *ACS Nano* **2014**, *8*, 4539−4546.
(46) Alligrant, T. M.; Anderson, M. J.; Dasari, R.; Stevenson, K. J.; Crooks, R. M. Single Nanoparticle Collisions at Microfluidic Microband Electrodes: The Effect of Electrode Material and Mass Transfer. *Langmuir* **2014**, *30*, 13462−13469.
(47) Alligrant, T. M.; Dasari, R.; Stevenson, K. J.; Crooks, R. M. Electrocatalytic Amplification of Single Nanoparticle Collisions Using DNA-Modified Surfaces. *Langmuir* **2015**, *31*, 11724−11733.
(48) Bigall, N. C.; Härtling, T.; Klose, M.; Simon, P.; Eng, L. M.; Eychmüller, A. Monodisperse Platinum Nanospheres with Adjustable Diameters from 10 to 100 nm: Synthesis and Distinct Optical Properties. *Nano Lett.* **2008**, *8*, 4588−4592.
(49) Perrin, D. D. *Ionisation Constants of Inorganic Acids and Bases in Aqueous Solution*; Pergamon Press: New York, 1982.
(50) Alfred, L. C. R.; Oldham, K. B. Steady-State Currents at Sphere-Cap Microelectrodes and Electrodes of Related Geometry. *J. Phys. Chem.* **1996**, *100*, 2170−2177.
(51) Clark, A. L. An Electric Heater and Automatic Thermostat. *Proc. Am. Acad. Arts Sci.* **1913**, *48*, 599−605.
(52) Hassan, M. Z.; Untereker, D. F.; Bruckenstein, S. Ring-Disk Study of Thin Mercury Films on Platinum. *J. Electroanal. Chem. Interfacial Electrochem.* **1973**, *42*, 161−181.

DOI: 10.1021/acs.jpclett.6b01131
J. Phys. Chem. Lett. 2016, 7, 2512−2517